Thruster Fault Detection, Isolation and Accommodation for an Autonomous Spacecraft

Robert Fonod, David Henry, Eric Bornschlegl, Catherine Charbonnel

Thruster Fault Detection, Isolation and Accommodation for an Autonomous Spacecraft [★]

R. Fonod [*] **D. Henry** [*] **E. Bornschlegl** [**] **C. Charbonnel** [***]

[*] *Université de Bordeaux, IMS UMR CNRS 5218, Talence, France*
{robert.fonod, david.henry}@ims-bordeaux.fr
[**] *European Space Agency, Noordwijk, The Netherlands*
[***] *Thales Alenia Space, Cannes, France*

Abstract: The presented work is a result of a research collaboration between European Space Agency, Thales Alenia Space and IMS Laboratory with the aim of promoting fault-tolerant control strategies to advance spacecraft autonomy. A multiple observer based scheme is proposed jointly with an online constrained allocation algorithm to detect, isolate and accommodate a single thruster fault affecting the propulsion system of an autonomous spacecraft. Robust residual generator with enhanced robustness to time delays induced by the propulsion drive electronics and uncertainties on thruster rise times is used for fault detection purposes. A decision test on the residual of the fault detector triggers a bank of nonlinear unknown input observers which is in charge of confining the fault to a subset of possible faults. The faulty thruster isolation is achieved by matching the residual and the thruster force directions using the direction cosine approach. Finally, the fault is accommodated by redistributing the desired forces and torques among the remaining (healthy) thrusters and closing the isolated thruster. Simulation results from the "high-fidelity" industrial simulator, provided by Thales Alenia Space, demonstrate the fault-tolerance capabilities of the proposed scheme.

1. INTRODUCTION

Space exploration missions require critical autonomous proximity operations. Mission safety is usually guaranteed via hierarchical implementation of Fault/Failure Detection, Isolation and Recovery (FDIR) approach (see for instance Olive [2012], Zolghadri [2012]). Fault detection and isolation are performed by simple cross checks between redundant units, limit checking, voting mechanisms, etc. Fixed thresholds are used for quick recognition of out-of-tolerance conditions. The recovery action is usually performed by switching to (hot) redundant units/strings (multiple sensors, actuators, processors, etc) or/and changing the operation mode to safe mode followed by ground intervention. Current FDIR techniques used in space systems are industrially well mastered, but may be not sufficient in some cases, specially for faulty situations causing quick and abnormal dynamics deviation in critical space operations. This is the case of thruster faults during terminal rendezvous and docking/capture phases, when a thruster failure could possibly lead to mission loss. Literature reports (see e.g. Wander and Förstner [2012]) that conventional FDIR methods are suffering from significant shortcomings, like often missing on-board fault isolation, increased mass and system complexity due to redundant equipment, ground intervention is not always possible as a result of large communication delays or visibility issues.

This motivates the European Space Agency (ESA) to manage studies for the development of fully autonomous on-board solutions that shall cope with all the possible faults that may occur and endanger the mission. Therefore, advanced Fault Detection and Isolation (FDI) approaches should be specifically developed to safely conjugate the necessary robustness/stability of the spacecraft control, trajectory dynamics and the vehicle nominal performance. Alternatively to redundancy-based FDIR techniques, model-based algorithms may offer a good balance between advanced strategies and existing physical redundancies that may lead to more efficient health monitoring and recovery systems based on fewer redundant components while providing large fault coverage capabilities.

In this paper, the application concerns the rendezvous phase of the Mars Sample Return (MSR) mission. The goal of this mission is to return samples from Mars to Earth for analysis. Obviously, the rendezvous phase might be endangered if a thruster fault occurs. As a consequence, the Guidance, Navigation, and Control (GNC) system may not fully compensate, for example, spatial disturbances, and/or may lose attitude, and/or the position of the sample container (target). This problem becomes highly critical during the last 20 meters of the rendezvous phase. During this phase, the chaser spacecraft must be correctly positioned in the approach corridor to successfully capture the target as well as the chaser's attitude need to be maintained in the rendezvous sensor' field of view.

Numerous model-based FDI techniques has been studied in the past decades in the academic community, see Blanke et al. [2006] and Ding [2008] for good surveys. The still

growing interest of potential applications in aerospace systems is demonstrated by recent publications, see, for instance, Chen and Saif [2007], Henry [2008], Patton et al. [2010], Falcoz et al. [2010], Posch et al. [2013]. In terms of fault accommodation techniques, the interested reader shall refer to literature review of Zhang and Jiang [2008].

The method introduced in this paper is sought from an industrial perspective. The aim is to develop an algorithm which can quickly detect, isolate, and accommodate single thruster fault in a simple manner and is easily implementable for a real spacecraft mission. As soon as a thruster is declared to be faulty by the FDI unit, the associated (faulty) thruster is closed by a dedicated thruster latch valve and the remaining (healthy) thrusters are used to control the spacecraft dynamics. This fault accommodation strategy is achieved by control re-allocation technique. By this way, the nominal (in-placed and certified) control law remains unchanged which is an important condition seen from an industrial point of view.

2. PROBLEM STATEMENT

The terminal rendezvous control mode corresponds to a 6 Degree of Freedom (DoF) control which ensures the application of both commanded force and torque vectors by means of thrusters only (reaction wheel control is turned off). The chaser spacecraft is equipped with a chemical propulsion system composed of $N = 12$ thrusters [1]. The thrusters are physically organised in four clusters and are in charge of producing force $\boldsymbol{F} \in \mathbb{R}^3$ and torque $\boldsymbol{T} \in \mathbb{R}^3$ vectors expressed in the chaser body-fixed reference frame $\mathcal{F}_b = \{O_b; \hat{\boldsymbol{x}}_b, \hat{\boldsymbol{y}}_b, \hat{\boldsymbol{z}}_b\}$. Let $\mathcal{S}_{all} = \{1, 2, \ldots N\}$ denote the set of all thruster indices. Thrusters have fixed directions $\boldsymbol{d}_i \in \mathbb{R}^3, \forall i \in \mathcal{S}_{all}$ and each one is able to produce a maximum thrust of $F_N = 22\text{N}$.

The Chemical Propulsion Drive Electronics (CPDE), that drives the thrusting actuators, is initiating the opening of the thruster valve for the commanded duration $0 \leq u_i(t) \leq 1, \forall i \in \mathcal{S}_{all}$. The propulsion system is obviously a source of uncertainty in the system. The irrational transfer

$$H(s) = e^{-\tau(t)s} \quad (1)$$

aims to model the effect of the unknown time-varying delays $\tau(t) \geq 0$ induced by the CPDE and the uncertainties on the thruster rise times. Let $u_i(t - \tau(t))$ be the commanded open rate of the ith thruster delayed by $\tau(t)$, then, the net forces and torques generated by the thrusters are

$$\boldsymbol{F}(t) = \boldsymbol{B}_F \boldsymbol{u}(t - \tau(t)), \quad \boldsymbol{T}(t) = \boldsymbol{B}_T \boldsymbol{u}(t - \tau(t)) \quad (2)$$

where $\boldsymbol{u}(t) = [u_1(t), \ldots, u_N(t)]^T$, and

$$\boldsymbol{B}_F = [\ \boldsymbol{b}_{F_1}\ \boldsymbol{b}_{F_2}\ \ldots\ \boldsymbol{b}_{F_N}\ ], \ \boldsymbol{B}_T = [\ \boldsymbol{b}_{T_1}\ \boldsymbol{b}_{T_2}\ \ldots\ \boldsymbol{b}_{T_N}\ ] \quad (3)$$

are the sensitivity (configuration) matrices. The columns of $\boldsymbol{B}_F$ and $\boldsymbol{B}_T$ are the influence coefficients defining how each thruster affects each component of $\boldsymbol{F}(t)$ and $\boldsymbol{T}(t)$, respectively, and are defined as follows

$$\boldsymbol{b}_{F_i} = -\boldsymbol{d}_i F_N, \ \boldsymbol{b}_{T_i} = (\boldsymbol{R}_i - \boldsymbol{R}_M) \times \boldsymbol{b}_{F_i}, \ \forall i \in \mathcal{S}_{all} \quad (4)$$

where " $\times$ " denotes the cross product, $\boldsymbol{R}_M \in \mathbb{R}^3$ is the position vector of the Center of Mass (CoM), and

$\boldsymbol{R}_i \in \mathbb{R}^3, \forall i \in \mathcal{S}_{all}$ are the position vectors of the thrusters, both expressed in the chaser body-fixed frame $\mathcal{F}_b$.

By analysing the configuration matrices $\boldsymbol{B}_F$ and $\boldsymbol{B}_T$ in terms of directional properties, the following can be concluded: thruster indices inside the sets $\mathcal{S}_{Ti}, i = 1, \ldots, 5$ have similar torque directions and are defined as

$$\begin{aligned} \mathcal{S}_{T1} &= \{1, 11\}, \ \mathcal{S}_{T3} = \{4, 8\}, \ \mathcal{S}_{T5} = \{3, 6, 9, 12\} \\ \mathcal{S}_{T2} &= \{2, 10\}, \ \mathcal{S}_{T4} = \{5, 7\}, \end{aligned} \quad (5)$$

In terms of force directions, the following is revealed

$$\begin{aligned} \boldsymbol{b}_{F_1} &= -\boldsymbol{b}_{F_{11}}, \ \boldsymbol{b}_{F_4} = -\boldsymbol{b}_{F_8}, \ \boldsymbol{b}_{F_3} = -\boldsymbol{b}_{F_{12}} \\ \boldsymbol{b}_{F_2} &= -\boldsymbol{b}_{F_{10}}, \ \boldsymbol{b}_{F_5} = -\boldsymbol{b}_{F_7}, \ \boldsymbol{b}_{F_6} = -\boldsymbol{b}_{F_9} \end{aligned} \quad (6)$$

which means that the thruster pairs given by $\mathcal{S}_{Ti}, i = 1, \ldots 4$ produce exactly opposite forces. The last thruster group, i.e. $\mathcal{S}_{T5}$, has the following orthogonal property

$$\boldsymbol{b}_{F_3} \cdot \boldsymbol{b}_{F_6} = 0, \ \ \boldsymbol{b}_{F_9} \cdot \boldsymbol{b}_{F_{12}} = 0 \quad (7)$$

where " $\cdot$ " denotes the dot product. Directional properties (5)-(7) will be used to derive an explicit isolation strategy.

The considered thruster faults are modeled in a multiplicative way according to (index "f" outlines the faulty case)

$$\boldsymbol{u}_f(t) = (\boldsymbol{I} - \boldsymbol{\Psi}(t))\boldsymbol{u}(t), \ \ \boldsymbol{\Psi}(t) = diag(\psi_1(t) \ldots \psi_N(t)) \quad (8)$$

where ψ_i models the health status of the ith thruster, i.e.

$$\psi_i(t) = \begin{cases} 0 & \text{if fault-free} \\ 1 - \phi_i(t)/u_i(t) & \text{if faulty} \end{cases} \quad (9)$$

ϕ_i allows to consider different fault scenarios. In this paper, we deal with the so-called "open-type" thruster faults:

$$\phi_i(t) = \begin{cases} 1 & \text{fully open thruster} \\ \max\{m_{leak}, u_i(t)\} & \text{propellant leakage} \end{cases} \quad (10)$$

where m_{leak} is the magnitude of the leaking thruster.

The two objectives addressed in this paper are:

(1) to quickly detect and isolate a single thruster fault while ensuring enhanced robustness to (1), and
(2) to accommodate this fault using the remaining $N - 1$ healthy thrusters so that the rendezvous criteria are met and the nominal controller remains in the loop.

3. FAULT DETECTION AND ISOLATION

The proposed model-based FDI scheme consists of a fault detector which is in charge of detecting the fault presence in the system. Once a detection flag is triggered, a bank of nonlinear Unknown Input Observers (UIOs) is used to identify the faulty thruster group that produce similar torques. In parallel to this, the fixed thruster force directions are compared with the residual generated by the fault detector. Subsequently, an isolation logic is used to make the final decision about the faulty thruster index.

3.1 Robust residual generator design

The proposed fault detector design is based on the relative position model of the chaser and target expressed in the local (target) frame $\mathcal{F}_l = \{O_l; \hat{\boldsymbol{x}}_l, \hat{\boldsymbol{y}}_l, \hat{\boldsymbol{z}}_l\}$. The interested reader can found further details on modeling the relative dynamics of two spacecrafts in the available space literature, see for instance Schaub and Junkins [2009]. Let a, m, $\mathcal{G}$, θ and m_M denote the orbit of the target, the mass of the chaser during rendezvous, the Mars gravitational constant,

---

[1] The considered thruster configuration in this paper is not a baseline MSR configuration, but a special one designed by Thales Alenia Space to study active fault tolerant control principles.

true anomaly and the mass of the planet. When the orbit of the rendezvous is circular, then the velocity of the chaser and the target is given by the relation $a\dot{\theta} = \sqrt{\mu/a}$ where $\mu = \mathcal{G}m_M$. From Kepler's third law it follows:

$$a\dot{\theta} = \sqrt{\mu/a} = \text{const.} \Rightarrow n = \sqrt{\mu/a^3} \qquad (11)$$

During the rendezvous phase, it is assumed that the chaser motion is due to the four following forces, all given in $\mathcal{F}_l$:

- the Mars attraction force
  $\boldsymbol{F}_a = -m\frac{\mu}{((a+x)^2+y^2+z^2)^{3/2}}\big((a+x)\hat{\boldsymbol{x}}_l + y\hat{\boldsymbol{y}}_l + z\hat{\boldsymbol{z}}_l\big)$
- the centripetal force $\boldsymbol{F}_e = m\left(n^2 x\hat{\boldsymbol{x}}_l + n^2 y\hat{\boldsymbol{y}}_l + 0\hat{\boldsymbol{z}}_l\right)$;
- the Coriolis force $\boldsymbol{F}_c = m\left(2n\dot{y}\hat{\boldsymbol{x}}_l - 2n\dot{x}\hat{\boldsymbol{y}}_l + 0\hat{\boldsymbol{z}}_l\right)$;
- and the non-gravitational (chemical thrust, perturbations) forces $\boldsymbol{F}_d = F_{dx}\hat{\boldsymbol{x}}_l + F_{dy}\hat{\boldsymbol{y}}_l + F_{dz}\hat{\boldsymbol{z}}_l$.

Then, from the 2nd Newton law, it follows

$$\ddot{x} = n^2(a+x) - \mu(a+x)\big((a+x)^2 + y^2 + z^2\big)^{-3/2}$$
$$\qquad + 2n\dot{y} + m^{-1}F_{dx}$$
$$\ddot{y} = n^2 y - 2n\dot{x} - \mu y\big((a+x)^2 + y^2 + z^2\big)^{-3/2} + m^{-1}F_{dy}$$
$$\ddot{z} = -\mu z\big((a+x)^2 + y^2 + z^2\big)^{-3/2} + m^{-1}F_{dz}$$

where x, y, z denote the elements of the three dimensional relative position vector of the chaser and target in $\mathcal{R}_l$. Because the distance between the target and the chaser during the rendezvous phase is much smaller than the orbit, it is possible to derive the so called Hill-Clohessy-Wiltshire (HCW) equations by means of a first order approximation. Hence, it follows a linear 6th order state space model with state vector $\boldsymbol{x}_p = [x\,y\,z\,\dot{x}\,\dot{y}\,\dot{z}]^T$ modelling the chaser relative motion expressed in $\mathcal{F}_l$, both in fault free (i.e. $\boldsymbol{\Psi} = \boldsymbol{0}$) and faulty (i.e. $\boldsymbol{\Psi} \neq \boldsymbol{0}$) situations, i.e.

$$\dot{\boldsymbol{x}}_p(t) = \boldsymbol{A}_p\boldsymbol{x}_p(t) + \boldsymbol{B}_p\boldsymbol{R}(\hat{\boldsymbol{q}}_t(t), \hat{\boldsymbol{q}}_c(t))\boldsymbol{B}_F\boldsymbol{u}_f(t-\tau(t)) \quad (12)$$
$$\boldsymbol{y}_p(t) = \boldsymbol{C}_p\boldsymbol{x}(t) \qquad (13)$$

where the rotation matrix $\boldsymbol{R}(\hat{\boldsymbol{q}}_t, \hat{\boldsymbol{q}}_c)$ is calculated from the quaternion estimates of the chaser $\hat{\boldsymbol{q}}_c \in \mathbb{H}$ and target $\hat{\boldsymbol{q}}_t \in \mathbb{H}$ attitude, and rotates the force vector from $\mathcal{F}_b$ into $\mathcal{F}_l$. These estimates come from the navigation. The output vector $\boldsymbol{y}_p = [x\,y\,z]^T$ is the relative position in $\mathcal{F}_l$ measured by a Light Detection and Ranging (LIDAR) device.

The position model given by (12) and (13) is well known and mastered for control, but rarely used for FDI purposes. The advantage is that this model takes into account both the rotational $\boldsymbol{q}_c$ and translational $\boldsymbol{x}$ motions of the chaser. Thus, effects that faults have on both the chaser attitude and translation are considered. Furthermore, this model is naturally robust against the model uncertainties, such as CoM and inertia, whilst the attitude model not. In Fonod et al. [2013a], a sensitivity/robustness analysis campaign was performed showing high reliability and efficiency (in terms of detection times) of a fault detector based on a position model in $\mathcal{F}_l$. Here, an observer-based fault detector is designed that has enhanced robustness to time-varying delay $\tau(t)$ introduced in (1). This observer exploits the position model given by (12) and (13) to generate the state estimate $\hat{\boldsymbol{x}}_p$ used to produce the residual signal $\boldsymbol{r} = [r_1, r_2, r_3]^T$ of the following form:

$$\boldsymbol{r}(t) = \boldsymbol{Q}\big(\boldsymbol{y}_p(t) - \boldsymbol{C}_p\hat{\boldsymbol{x}}_p(t)\big) \qquad (14)$$

where $\boldsymbol{Q}$ is a weighting matrix. The design of (14) is based on theoretical developments given in Fonod et al. [2013b].

3.2 Decision test: fault detection

The proposed decision test is motivated by the scalar valued Generalized Likelihood Ratio (GLR) test given in Ding [2008], i.e.

$$S_i(k) = N_d\ln(\sigma_i) - \frac{N_d}{2}\left(1 + \ln(\hat{\sigma}_i^2(k)) - \frac{\hat{\sigma}_i^2(k)}{\sigma_i^2}\right) \quad (15)$$

$$\hat{\sigma}_i^2(k) = \frac{1}{N_d}\sum_{j=k-N_d+1}^{k} r_i^2(j) \qquad (16)$$

where $r_i(k)$ is the ith element of the residual $\boldsymbol{r}(k)$ evaluated at time instant $t = kT_s$, $k = 0, 1, 2, \ldots$ where T_s is the navigation sampling time, σ_i is the (fixed) standard deviation of r_i in fault free situation and $N_d > 1$ represents the detection sliding window due to on-line realization. The proposed decision test $\rho(t)$ is defined by

$$\rho(t) = \begin{cases} 1, & S(k) > J_{th} \Rightarrow \text{fault declared} \\ 0, & S(k) \leq J_{th} \Rightarrow \text{fault not present} \end{cases} \quad (17)$$

where J_{th} is a fixed threshold selected by the designer and $S(k)$ is given by

$$S(k) = \sum_{j=1}^{3} w_j S_j(k), \quad \sum_{j=1}^{3} w_j = 1 \qquad (18)$$

where $w_j \geq 0$, $j = 1, 2, 3$ are the weight factors used to prioritize certain elements (axis) of the residual.

3.3 Nonlinear unknown input observer

We will briefly state the main results obtained in Chen and Saif [2006]. Considering the following nonlinear system

$$\dot{\boldsymbol{x}}(t) = \boldsymbol{A}\boldsymbol{x}(t) + \boldsymbol{B}\boldsymbol{u}(t) + \boldsymbol{f}(\boldsymbol{x}(t)) + \boldsymbol{E}\boldsymbol{d}(t) \qquad (19)$$
$$\boldsymbol{y}(t) = \boldsymbol{C}\boldsymbol{x}(t) \qquad (20)$$

where $\boldsymbol{x} \in \mathbb{R}^n$ stands for the state vector, $\boldsymbol{y} \in \mathbb{R}^m$ is the output, $\boldsymbol{u} \in \mathbb{R}^r$ is the input, $\boldsymbol{d} \in \mathbb{R}^q$ is the unknown input (disturbance) vector, and $\boldsymbol{f}(\boldsymbol{x}) \in \mathbb{R}^n$ is a known nonlinear vector function of $\boldsymbol{x}$ satisfying:

$$\|\boldsymbol{f}(\boldsymbol{x}_1) - \boldsymbol{f}(\boldsymbol{x}_2)\| \leq \kappa\|\boldsymbol{x}_1 - \boldsymbol{x}_2\|, \quad \forall \boldsymbol{x}_1, \boldsymbol{x}_2 \in \mathbb{R}^n \quad (21)$$

where $\kappa > 0$ stands for the Lipschitz constant.

The goal is to design an asymptotically converging state observer to estimate $\boldsymbol{x}$ in the presence of an unknown input $\boldsymbol{d}$. A nonlinear UIO for the system (19)-(20) achieving this goal has the following structure

$$\dot{\boldsymbol{z}}(t) = \boldsymbol{N}\boldsymbol{z}(t) + \boldsymbol{G}\boldsymbol{u}(t) + \boldsymbol{L}\boldsymbol{y}(t) + \boldsymbol{M}\boldsymbol{f}(\hat{\boldsymbol{x}}(t)) \qquad (22)$$
$$\hat{\boldsymbol{x}}(t) = \boldsymbol{z}(t) - \boldsymbol{H}\boldsymbol{y}(t) \qquad (23)$$

where $\hat{\boldsymbol{x}} \in \mathbb{R}^n$ is an estimate of $\boldsymbol{x}$, $\boldsymbol{z} \in \mathbb{R}^n$ is an auxiliary signal and the matrices $\boldsymbol{N}$, $\boldsymbol{G}$, $\boldsymbol{L}$, $\boldsymbol{M}$ are designed as in Chen and Saif [2006]:

$$\boldsymbol{N} = \boldsymbol{M}\boldsymbol{A} - \boldsymbol{K}\boldsymbol{C}, \quad \boldsymbol{G} = \boldsymbol{M}\boldsymbol{B} \qquad (24)$$
$$\boldsymbol{L} = \boldsymbol{K}(\boldsymbol{I} + \boldsymbol{C}\boldsymbol{H}) - \boldsymbol{M}\boldsymbol{A}\boldsymbol{H} \qquad (25)$$
$$\boldsymbol{M} = \boldsymbol{I} + \boldsymbol{H}\boldsymbol{C} \qquad (26)$$

$\boldsymbol{K}$ and $\boldsymbol{H}$ being designed subsequently.

Without loss of generality, it is assumed that $\boldsymbol{E}$ is of full column rank. The necessary condition for $\boldsymbol{H}\boldsymbol{C}\boldsymbol{E} = -\boldsymbol{E}$ to have solution is that $\boldsymbol{C}\boldsymbol{E}$ is also of full column rank and the solution is given in a generalized form by

$$\boldsymbol{H} = \boldsymbol{U} + \boldsymbol{Y}\boldsymbol{V} \qquad (27)$$

where $\boldsymbol{Y}$ can be chosen arbitrarily, $\boldsymbol{U}$ and $\boldsymbol{V}$ are given by

$$\boldsymbol{U} = -\boldsymbol{E}(\boldsymbol{CE})^+, \quad \boldsymbol{V} = \boldsymbol{I} + (\boldsymbol{CE})(\boldsymbol{CE})^+ \qquad (28)$$

and $(\boldsymbol{CE})^+$ denotes the generalized pseudo-inverse of the matrix $\boldsymbol{CE}$ given by $(\boldsymbol{CE})^+ = ((\boldsymbol{CE})^T(\boldsymbol{CE}))^{-1}(\boldsymbol{CE})^T$.

Theorem 1. (Chen and Saif [2006]). Assume that $\boldsymbol{CE}$ is of full column rank and that the following Linear Matrix Inequality (LMI)

$$\begin{bmatrix} \boldsymbol{X} & \boldsymbol{X}_{12} \\ \boldsymbol{X}_{12}^T & -\boldsymbol{I} \end{bmatrix} < 0 \qquad (29)$$

where $\boldsymbol{X}$ and $\boldsymbol{X}_{12}$ are defined as

$$\boldsymbol{X} = [(\boldsymbol{I} + \boldsymbol{UC})\boldsymbol{A}]^T \boldsymbol{P} + \boldsymbol{P}(\boldsymbol{I} + \boldsymbol{UC})\boldsymbol{A} - \boldsymbol{C}^T \bar{\boldsymbol{K}}^T$$
$$- \bar{\boldsymbol{K}}\boldsymbol{C} + (\boldsymbol{VCA})^T \bar{\boldsymbol{Y}}^T + \bar{\boldsymbol{Y}}(\boldsymbol{VCA}) + \kappa \boldsymbol{I}$$
$$\boldsymbol{X}_{12} = \sqrt{\kappa}[\boldsymbol{P}(\boldsymbol{I} + \boldsymbol{UC}) + \bar{\boldsymbol{Y}}(\boldsymbol{VC})]$$

has a feasible solution for $\bar{\boldsymbol{Y}}$, $\bar{\boldsymbol{K}}$ and $\boldsymbol{P} = \boldsymbol{P}^T > 0$, then the nonlinear UIO given by (22) and (23) can be designed with $\boldsymbol{Y} = \boldsymbol{P}^{-1}\bar{\boldsymbol{Y}}$, and $\boldsymbol{K} = \boldsymbol{P}^{-1}\bar{\boldsymbol{K}}$ making $\boldsymbol{N}$ being Hurwitz and the estimation error $\boldsymbol{e}(t) = \hat{\boldsymbol{x}}(t) - \boldsymbol{x}(t)$ tending to zero asymptotically for any initial value of $\boldsymbol{e}(0)$.

Proof. The proof can be found in Chen and Saif [2006].

3.4 Thruster group isolation: a bank of nonlinear UIOs

Recalling the thruster configuration properties given by (5)-(7), we assume, that for fault isolation it is easier to obtain explicit information from the angular velocity $\boldsymbol{\omega} \in \mathbb{R}^3$ measurement than from the linear position/velocity. Therefore, the below model of the attitude dynamics of a rigid-body spacecraft in the body-fixed frame $\mathcal{F}_b$

$$\boldsymbol{J}\dot{\boldsymbol{\omega}}(t) = \boldsymbol{B}_T \boldsymbol{u}_f(t) - \boldsymbol{\omega}(t) \times \boldsymbol{J}\boldsymbol{\omega}(t) \qquad (30)$$

is used for the design of a bank of UIOs. In (30), $\boldsymbol{J} \in \mathbb{R}^{3 \times 3}$ stands for the inertia of the chaser in $\mathcal{F}_b$. A nonlinear UIO, as introduced in section 3.3, has been selected because of its decoupling properties and the ability to take into account nonlinearities of the attitude dynamics.

The attitude model (30) can be represented in the form of (19) and (20) with the following assignment: $\boldsymbol{x} = \boldsymbol{\omega}$, $\boldsymbol{f}(\boldsymbol{\omega}) = -\boldsymbol{J}^{-1}\boldsymbol{\omega} \times \boldsymbol{J}\boldsymbol{\omega}$, $\boldsymbol{A} = 0$, $\boldsymbol{B} = \boldsymbol{J}^{-1}\boldsymbol{B}_T$, and $\boldsymbol{C} = \boldsymbol{I}$. One may argue that $\boldsymbol{f}(\boldsymbol{\omega})$ is not globally Lipschitz, because the Jacobian $\partial \boldsymbol{f}/\partial \boldsymbol{\omega}$ is not uniformly bounded over $\mathbb{R}^3$. However, $\boldsymbol{f}(\boldsymbol{\omega})$ is continuously differentiable on $\mathbb{R}^3$. Thus, it is locally Lipschitz. This means that the angular velocity shall be bounded in magnitude which is a reasonable assumption from a practical point of view. Using a constrained optimization algorithm, one can find a Lipschitz constant κ over the set $\mathcal{S} = \{\boldsymbol{\omega} \in \mathbb{R}^3 : |\omega_i| \leq \bar{\omega}_i, \; i = 1, 2, 3\}$, where $\bar{\omega}_i > 0$ is the upper bound of the angular velocity in the given axis.

For each thruster group $\mathcal{S}_{Ti}$, a dedicated UIO is designed. Each UIO is such that it can fully estimate the angular velocity $\boldsymbol{\omega}$ with all the inputs except those belonging to $\mathcal{S}_{Ti}$, i.e. $u_i, \; i \in \mathcal{S}_{all} \backslash \mathcal{S}_{Ti}$. As a result, the UIO dedicated to the thruster group $\mathcal{S}_{Ti}$ will not be influenced by faults occurring in thrusters that belong to $\mathcal{S}_{Ti}$, while all the other UIOs will be. Based on Theorem 1, the design of a bank of nonlinear UIOs is summarized in Algorithm 1.

The ith observer only estimates the angular velocity $\hat{\boldsymbol{\omega}}_i$ of the chaser from the measurement $\boldsymbol{\omega}$. Therefore, the compu-

---

Algorithm 1 Bank of nonlinear UIO design

Find a Lipschitz constant κ satisfying (21);
for $k = 1$ to 5 **do**
  Construct $\boldsymbol{B}_k^\star$ whose columns are $\boldsymbol{b}_{Ti}$, $\forall i \in \mathcal{S}_{all} \backslash \mathcal{S}_{Tk}$;
  Set $\boldsymbol{E} = \boldsymbol{b}_{Ti}$ for any arbitrary $i \in \mathcal{S}_{Tk}$ and $\boldsymbol{B} = \boldsymbol{B}_k^\star$;
  Compute $\boldsymbol{U}$ and $\boldsymbol{V}$ according to (28);
  Solve the LMI defined by (29) for $\bar{\boldsymbol{Y}}$, $\bar{\boldsymbol{K}}$ and $\boldsymbol{P} = \boldsymbol{P}^T > 0$;
  Let $\boldsymbol{Y} = \boldsymbol{P}^{-1}\bar{\boldsymbol{Y}}$ and $\boldsymbol{K} = \boldsymbol{P}^{-1}\bar{\boldsymbol{K}}$;
  Using $\boldsymbol{Y}$ and $\boldsymbol{K}$, the kth UIO gains are given by (24)-(27);
end for

---

tational burden is reduced since there is no need to process the entire state vector (i.e. the linear position/velocity and attitude in addition). For real-time reasons, the UIOs are triggered only when $\rho(t)$ indicates that a fault has been occurred. Even if only $\boldsymbol{\omega}$ is estimated, keeping the UIOs switched off before the fault is detected seems to be a good strategy, regarding the nonlinear nature of the observer. Let t_d denote the fault detection time, i.e. the time when the fault is declared by $\rho(t)$, and $\mathcal{D} = \{1, 2, ...5\}$ the set of all indices linked with the thruster groups $\mathcal{S}_{T1}, ..., \mathcal{S}_{T5}$. Each observer is initialized with the (known) measurement at time t_d, i.e. $\hat{\boldsymbol{\omega}}_i(t_d) = \boldsymbol{\omega}(t_d)$, $\forall i \in \mathcal{D}$. By this, all observers have zero initial estimation error. Hence, the observer initial convergence (transient phase) problem is avoided.

Defining the angular velocity estimation error of the ith observer as $\boldsymbol{e}_i(t) = \hat{\boldsymbol{\omega}}_i(t) - \boldsymbol{\omega}(t)$, then the faulty thruster group $\mathcal{S}_{Ti}$ is identified based on the following rule

$$\sigma_g(t) = \arg \min_{i \in \mathcal{D}} \|\boldsymbol{e}_i(t)\|, \quad t > t_d \qquad (31)$$

where $\sigma_g(t) : \mathbb{R}^+ \to \mathcal{D}$ represents the identified thruster group index that is most likely affected by a fault.

Remark 1. It is assumed that the time-varying delay (1) has no big effect on the isolation performance. Therefore, $\tau(t)$ is not considered in (30). Furthermore, the isolation process is triggered by the decision test $\rho(t)$ which already has enhanced robustness to $\tau(t)$.

3.5 Isolation logic

Once the thruster group $\mathcal{S}_{Ti}$ is identified by σ_g, the faulty thruster can be easily isolated by examining the angle of the vector $\boldsymbol{r}$ given by (14) along the force directions $\boldsymbol{b}_{Fi}, \; i \in \mathcal{S}_{Ti}$. When the ith thruster is faulty, then vectors $\boldsymbol{r}$ and $\boldsymbol{b}_{Fi}$ should be collinear. The degree of collinearity can be computed using the direction cosine approach: $\cos(\theta_i(t)) = \boldsymbol{b}_{Fi}^T \boldsymbol{r}(t)/(\|\boldsymbol{b}_{Fi}\| \|\boldsymbol{r}(t)\|)$, where θ_i is the angle between the vectors $\boldsymbol{r}$ and $\boldsymbol{b}_{Fi}$. If $\boldsymbol{r}$ and $\boldsymbol{b}_{Fi}$ are collinear, then $\cos(\theta_i) = 1$ (and the angle between the two vectors $\theta_i = 0$). Thus, the following isolation logic

$$\sigma(t) = \arg \max_{j \in \mathcal{S}_{Ti}} \frac{\boldsymbol{b}_{Fj}^T \boldsymbol{r}(t)}{\|\boldsymbol{b}_{Fj}\| \|\boldsymbol{r}(t)\|} \qquad (32)$$

results in the thruster index matching the faulty thruster. This isolation logic has to clearly indicate which actuator is faulty. Therefore, only thrusters belonging to the (already) identified group $\mathcal{S}_{Ti}$ are tested in (32). Since the force directions within the groups $\mathcal{S}_{Ti}, i \in \mathcal{D}$ are either exactly opposite, see (6), or are orthogonal, see (7), it makes the isolation logic $\sigma(t) : \mathbb{R}^+ \times \mathcal{D} \to \mathcal{S}_{all}$ very reliable.

To avoid initial transition phenomena and to ensure robustness, we introduce two confirmation windows $\delta_g > 0$ for $\sigma_g(t)$ and $\delta > 0$ for $\sigma(t)$. The whole fault detection and isolation strategy is summarised in Algorithm 2.

Algorithm 2 Thruster fault detection and isolation

if $\rho(t) = 1$ **then**

  Decision = Declare a fault presence and run the UIOs;

  if $\sigma_g(t) = \sigma_g(\nu)$, $\forall \nu \in (t - \delta_g, t]$ **then**

    Decision = The faulty thruster group $\mathcal{S}_{Ti}$ is identified;

    if $\sigma(t) = \sigma(\nu)$, $\forall \nu \in (t - \delta, t]$ **then**

      Decision = Declare the $i^{th} = \sigma(t)$ thruster to be faulty

end all if

4. FAULT ACCOMMODATION

In the investigated thruster configuration, an additional freedom is available to achieve fault tolerance. Particularly, it means that it is possible to achieve admissible GNC performance even if only $N-1$ (healthy) thrusters are used to control the spacecraft. The nominal 6DOF control law is designed based on certain predetermined performance criteria. Hence, after the fault occurrence, it is desirable to keep the nominal controller in the loop and perform the fault accommodation on the control allocation level which can counteract the effect of the fault in a simple manner.
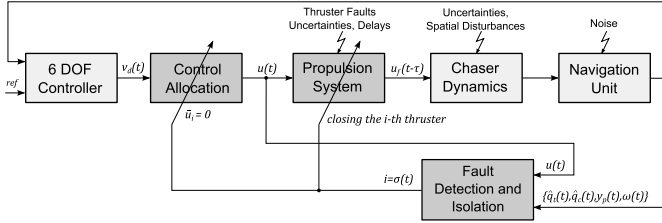

Fig. 1. Principal accommodation scheme for thruster faults

Figure 1 illustrates the proposed Fault Detection, Isolation and Accommodation (FDI-A) scheme implemented within the GNC system. The FDI-A strategy works as follows: as soon as the faulty thruster index is clearly isolated by Algorithm 2, the faulty thruster is switched off using a dedicated thruster latch valve and the desired forces and torques are re-allocated among the remaining $N-1$ healthy thrusters. Here, the quadratic programming approach, also known as l_2-optimal control allocation, is used. This problem is posed as the following Sequential Least-Squares (SLS) problem:

$$\boldsymbol{u} = \arg \min_{\boldsymbol{u} \in \mathcal{M}} \|\boldsymbol{W}_u(\boldsymbol{u} - \boldsymbol{u}_d)\| \qquad (33)$$

$$\mathcal{M} = \arg \min_{\boldsymbol{0} \leq \boldsymbol{u} \leq \bar{\boldsymbol{u}}} \|\boldsymbol{W}_v(\boldsymbol{B}_a\boldsymbol{u} - \boldsymbol{v}_d)\| \qquad (34)$$

where $\boldsymbol{B}_a^T = [\boldsymbol{B}_F^T \ \boldsymbol{B}_T^T]$ is the overall configuration matrix, $\boldsymbol{v}_d$ is the augmented vector of the desired forces and torques, $\bar{\boldsymbol{u}} = [\bar{u}_1, ..., \bar{u}_{12}]^T$ are the upper limits defined as: $\bar{u}_i = 1, \forall i \in \mathcal{S}_{all} \backslash \sigma(t)$ and $\bar{u}_i = 0$, $i = \sigma(t)$. This optimization problem should be understood as follows: given $\mathcal{M}$, the set of feasible control inputs minimizing $\boldsymbol{B}_a\boldsymbol{u} - \boldsymbol{v}_d$ (weighted by $\boldsymbol{W}_v$), pick the control input that minimize $\boldsymbol{u} - \boldsymbol{u}_d$ (weighted by $\boldsymbol{W}_u$). Here, $\boldsymbol{u}_d$ is the desired control input and $\boldsymbol{W}_u$ and $\boldsymbol{W}_v$ are nonsingular weighting matrices. $\boldsymbol{W}_u$ affects the control distribution among the thrusters and $\boldsymbol{W}_v$ affects the prioritization among force/torque components when $\boldsymbol{B}_a\boldsymbol{u} - \boldsymbol{v}_d$ cannot be attained due to, e.g. thruster constraints. A faster algorithm can be obtained by approximating the SLS formulation as a Weighted Least-Squares (WLS) problem:

$$\min \|\boldsymbol{W}_u(\boldsymbol{u} - \boldsymbol{u}_d)\|^2 + \gamma \|\boldsymbol{W}_v(\boldsymbol{B}_a\boldsymbol{u} - \boldsymbol{v}_d)\|^2$$
$$\text{subj. to } \ \boldsymbol{0} \leq \boldsymbol{u} \leq \bar{\boldsymbol{u}} \qquad (35)$$

As $\gamma \to \infty$, the two formulations have the same optimal solution $\boldsymbol{u}$. The cost function (35) may be re-written as

$$\|\boldsymbol{W}_u(\boldsymbol{u} - \boldsymbol{u}_d)\|^2 + \gamma \|\boldsymbol{W}_v(\boldsymbol{B}_a\boldsymbol{u} - \boldsymbol{v}_d)\|^2$$
$$= \Big\| \underbrace{\begin{pmatrix} \sqrt{\gamma}\boldsymbol{W}_v\boldsymbol{B}_a \\ \boldsymbol{W}_u \end{pmatrix}}_{\boldsymbol{A}^\circ} \boldsymbol{u} - \underbrace{\begin{pmatrix} \sqrt{\gamma}\boldsymbol{W}_v\boldsymbol{v}_d \\ \boldsymbol{W}_u\boldsymbol{u}_d \end{pmatrix}}_{\boldsymbol{b}^\circ} \Big\|^2 \qquad (36)$$

allowing the minimization problem to be formulated as

$$\min \|\boldsymbol{A}^\circ\boldsymbol{u} - \boldsymbol{b}^\circ\|^2, \text{ subj. to } \boldsymbol{0} \leq \boldsymbol{u} \leq \bar{\boldsymbol{u}} \qquad (37)$$

which can be solved using an active set algorithm, see Härkegård [2002] for implementation details. This algorithm determines the optimal solution in a finite number of iterations. The max number of iteration N_{ca} can be considered to reflect the max computation time available.

5. SIMULATION RESULTS

The FDI-A scheme described in the previous sections is implemented within the MSR "high-fidelity" industrial simulator. Following the design steps given in Algorithm 1, a bank of 5 nonlinear observers were designed with $\kappa = 0.2$. The WLS control allocation algorithm presented in section 4 was implemented using $\boldsymbol{W}_v = \boldsymbol{I}$, $\boldsymbol{W}_u = \boldsymbol{I}$, $\boldsymbol{u}_d = \boldsymbol{0}$, $N_{ca} = 100$, and $\gamma = 100$. The remaining design parameters were chosen as follows: $\boldsymbol{Q} = \boldsymbol{I}$, $N_d = 10$, $J_{th} = 200$, $T_s = 0.1$, $w_i = 1/3, \forall i \in \{1, 2, 3\}$, $\delta_g = 0.5$, and $\delta = 0.5$. The simulation examples are all carried out during the last 20m of the rendezvous phase. The navigation unit is assumed to be decoupled from thruster faults, but providing noisy estimates. We also assume delays induced by the CPDE device, uncertainties on thruster rise times, uncertain mass, Inertia, CoM (thus uncertain $\boldsymbol{B}_T$) and spatial disturbances (i.e. gravity gradient, atmospheric drag, and solar radiation pressure).
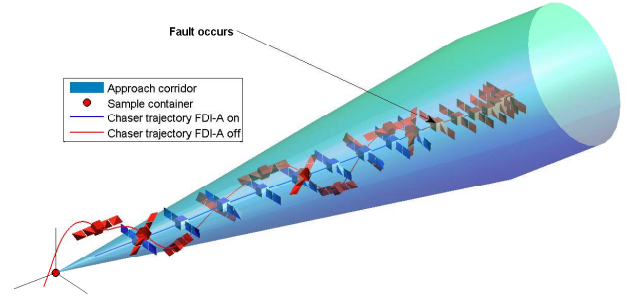

Fig. 2. MSR rendezvous corridor

The first fault scenario corresponds to a fully open thruster fault (thruster provides maximum thrust regardless of the control signal) occurring at $t_f = 1100s$ and affecting thruster No.7. To emphasize the relevance of the engagement of the proposed scheme into the GNC system, two identical simulations are carried out. First, when the FDI-A scheme is active (FDI-A on), and second, when not (FDI-A off). Figure 2 clearly illustrates the consequence when the fault is not accommodated, i.e. chaser miss the target and the mission is lost. On the other hand, when the proposed approach is active, the chaser maintains nominal trajectory, i.e. stays inside the rendezvous corridor and the MSR capture requirements are met, see Fig.3. Furthermore, it can be inferred from Fig.2 that the chaser keeps its attitude pointing towards the target. Hence, the target remains visible from the rendezvous sensors.
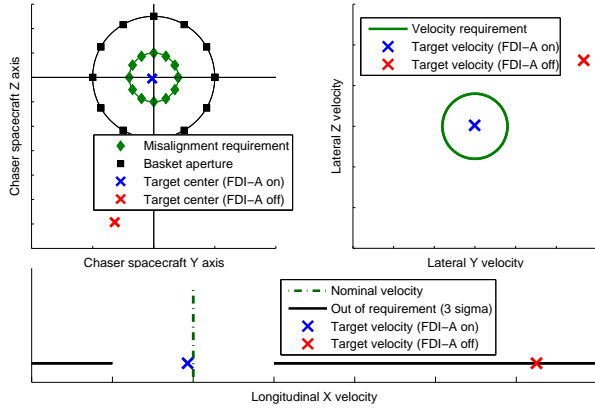
Fig. 3. MSR capture performance: position misalignment on +X face (top left), lateral velocity (top right) and longitudinal velocity (bottom) requirements
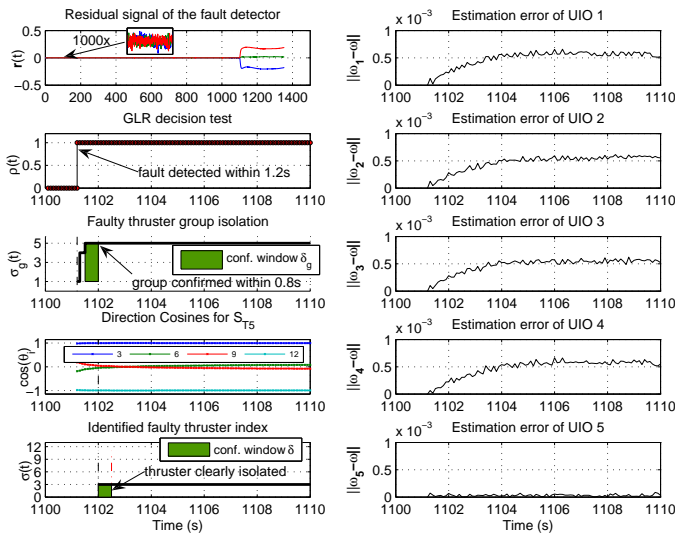

Fig. 4. Fault detection and isolation algorithm behaviour

Figure 4 aims to illustrate the time behaviour of the FDI algorithm for the second fault scenario which corresponds to a leaking thruster of size $m_{leak} = 15\%$ and affecting thruster No.3 from $t_f = 1100s$. This fault is maintained during the whole length of the simulation and is not accommodated. The fault presence is declared at $t_d = 1101.2s$ and the faulty thruster index clearly isolated at $t_i = 1102.5s$. As it can be seen from Fig.4, despite the small leakage size, external disturbances and uncertainties, the right thruster index was isolated in a reasonable time.

6. CONCLUSIONS

In this paper, a method to unambiguously detect, isolate and accommodate a single "open-type" thruster fault of an autonomous spacecraft has been studied. The method differs from the usual solutions by the use of two observers, one for detection and one for thruster group isolation. Time delays induced by the propulsion drive electronic and uncertainties on thruster rise times have been considered on the detection level. Finally, when a thruster is clearly isolated, the faulty thruster is turned off and the remaining $N-1$ healthy thrusters are used. This makes the fault accommodation without any change in the nominal con-troller (GNC system), requiring any redundant thruster set or any additional valve position sensor. This is in contrast to the classical FDIR approach, used in the satellite systems, where fault isolation is not always possible.

REFERENCES

M. Blanke, M. Kinnaert, J. Lunze, and M. Staroswiecki. *Diagnosis and Fault-Tolerant Control*. Springer, 2006.

W. Chen and M. Saif. Unknown input observer design for a class of nonlinear systems: an LMI approach. In *Proc. of American Control Conference*, pages 834–Ű838, Minneapolis, USA, 2006.

W. Chen and M. Saif. Observer-based fault diagnosis of satellite systems subject to time-varying thruster faults. *Journal of Dynamic Systems, Measurement and Control*, 129(3):352–356, 2007.

S.X. Ding. *Model-based fault diagnosis techniques: design schemes, algorithms, and tools*. Springer Verlag, 2008.

A. Falcoz, F. Boquet, M. Dinh, B. Polle, G. Flandin, and E. Bornschlegl. Robust fault diagnosis strategies for spacecraft application to LISA pathfinder experiment. In *Proc. of IFAC Symposium on Automatic Control in Aerospace*, pages 404–409, 2010.

R. Fonod, D. Henry, E. Bornschlegl, and C. Charbonnel. Robust fault detection for systems with electronic induced delays: Application to the rendezvous phase of the MSR mission. In *Proc. of European Control Conference*, pages 1439–1444, Zürich, Switzerland, 2013a.

R. Fonod, D. Henry, C. Charbonnel, and E. Bornschlegl. Robust thruster fault diagnosis: Application to the rendezvous phase of the Mars Sample Return mission. In *Proc. of CEAS Specialist Conference on Guidance, Navigation and Control*, pages 1496–1510, Delft, NL, 2013b.

Ola Härkegård. Efficient active set algorithms for solving constrained least squares problems in aircraft control allocation. In *Proc. of Conference on Decision and Control*, pages 1295–1300, Las Vegas, NV, 2002.

D. Henry. Fault diagnosis of microscope satellite thrusters using H_∞/H_- filters. *Journal of Guidance, Control, and Dynamics*, 31(3):699–711, 2008.

X. Olive. FDI(R) for satellites: How to deal with high availability and robustness in the space domain? *International Journal of Applied Mathematics and Computer Science*, 22(1):99–107, 2012.

R. Patton, F. Uppal, S. Simani, and B. Polle. Robust FDI applied to thruster faults of a satellite system. *Control Engineering Practice*, 18(9):1093–1109, 2010.

A. Posch, A.O. Schwientek, J. Sommer, and W. Fichter. Model-based on-board realtime thruster fault monitoring. In *Proc. of IFAC Symposium on Automatic Control in Aerospace*, pages 553–558, Würzburg, Germany, 2013.

H. Schaub and J.L. Junkins. *Analytical Mechanics of Space Systems*. AIAA Education Series, Reston, VA, 2009.

A. Wander and R. Förstner. Innovative fault detection, isolation and recovery strategies on-board spacecraft: State of the art and research challenges. In *Proc. of Deutscher Luft- und Raumfahrkongress*, Berlin, 2012.

Y. Zhang and J. Jiang. Bibliographical review on reconfigurable fault-tolerant control systems. *Annual Reviews in Control*, 32(2):229–252, 2008.

A. Zolghadri. Advanced model-based FDIR techniques for aerospace systems: Today challenges and opportunities. *Progress in Aerospace Sciences*, 53(3):18–29, 2012.